Electronic-structure-based pair potentials for aluminum-rich cobalt compounds

Rob Phillips*

Laboratory of Atomic and Solid-State Physics, Clark Hall, Cornell University, Ithaca, New York 14853

J. Zou† and A. E. Carlsson

Department of Physics, Washington University, St. Louis, Missouri 63130-4899

M. Widom

Department of Physics, Carnegie Mellon University, Pittsburgh, Pennsylvania 15213

A method for calculating "constant volume" pair potentials in Al-rich transition-metal compounds is presented. The method is based on a combination of a Green's-function analysis of the interaction between transition-metal d shells, and a perturbative treatment of the Al and transition-metal pseudopotentials. In addition to the d-shell interactions, the pair potentials include terms describing interactions between pseudopotentials on different atoms, as well as interactions between the pseudopotential on one atom and the charge density induced by the d shell on another atom. The potentials are parametrized by use of both *ab initio* total-energy results and experimental inputs. The methodology is tested by calculating the energies of many different structures at the Al-rich end of the Al-Co phase diagram. The potentials correctly predict the sequence of complex phases that occurs with increasing Co content, with just one exception. The complex phases are favored relative to simpler fcc-based phases by a large energy due mainly to short-ranged spacing constraints. The Co-Co potential has a secondary minimum at 4.4 Å which coincides with the Co-Co spacings in the complex structures, and thus further enhances their stability.

I. INTRODUCTION

The aim of this paper is to describe and illustrate a methodology for calculating potential-energy functions in Al-rich transition-metal compounds. Such compounds are of interest for two reasons. First, and most directly related to the results of this paper, such compounds often form quasicrystalline and related complex structures. The first observations of quasicrystallinity were in the Al-Mn system,[1] at around 20% Mn. Subsequently many additional binary and ternary quasicrystals have been discovered in the Al-rich aluminides, with the ternary ones AlCuFe and AlCuCo being particularly stable.[2-4] It is hoped that the development of increasingly accurate potential-energy functions can aid our understanding of the quasicrystal phenomenon, both through the elucidation of general bonding constraints, as well as through direct atomic simulations of solidification processes. Second, Al-rich aluminides have considerable technological promise because of their combination of hardness, light weight, and high melting points. However, they have typically suffered from brittleness problems. Understanding and perhaps remedying the brittleness will involve atomistic simulations of grain boundaries, dislocations, and cracks. Only the simplest of these can be treated via existing *ab initio* methods, so that reliable potentials for these systems will be of great importance.

Aside from purely empirical pair-potential models, two types of potential-energy functions have been developed for the Al-rich aluminides. The first is based on the embedded-atom method (EAM),[5-7] in which the energy of a system is divided into individual atomic contributions, each of which is given as a nonlinear function of a "background electron density" at the position of its nucleus. The background electron density is in turn given as a sum of pair contributions from the neighboring atoms, using atomic electron densities that have an exponential decay. Because the energy function is nonlinear, the method effectively includes many-atom interactions. The exponential decay renders these short ranged, making this method very computationally tractable. The main problem with application of EAM-type methods to, for example, dislocation structure, is that they typically yield structural-energy differences which are much too small.[7,8] This in turn likely causes underestimates of the energies of planar defects, such as stacking faults and antiphase-boundary energies. Since these planar-defect energies directly enter the dissociation of dislocations, the dislocation structure may well be inaccurate. Of course, one can fit the parameters in the method to known planar-defect energies, but usually not enough of these numbers are known to completely determine the dislocation structure.

The second type of potential-energy function that has been developed for the Al-rich aluminides[9] is based on interactions between the transition-metal d shells, mediated by the Al free-electron sea; the latter is modeled as a uniform gas. This approach is similar in spirit to that of Moriarty[10,11] for transition metals. The transition-metal–transition-metal (T-T) interactions are calculated using a Green's-function methodology. They have a strong long-range oscillatory behavior, which leads to

large structural-energy differences. Chemical trends in structural energies result from variations in the phase and magnitude of the T-T interactions. For the benchmark $DO_{22}-L1_2$ energy difference, the T-T interactions give quite accurate results for middle transition metals. These types of potentials are incomplete, because the Al-Al and Al-T interactions have not yet been evaluated.

In this paper, we extend the latter method to obtain a complete set of potentials which can be used for atomistic simulations. The main additional ingredients are atomic pseudopotentials for both Al and T, which scatter the free electrons, as well as repulsive Coulomb interactions between the nuclei. This results in two types of additional pair-potential terms. The first is the familiar interaction between pseudopotentials on different sites,[12] obtained by treating the pseudopotentials to second order, using the electron-gas response function for a uniform electron gas. The second type of term involves the interaction between the pseudopotential on one site (either Al or T) and the d-induced charge on another T site. This interaction is obtained in the obvious fashion by simply integrating the pseudopotential with the induced charge. We ignore direct d-hopping-type interactions between the T atoms.

To illustrate the methodology, we use the Al-Co system. This choice is made for three reasons. First, the AlCo system exhibits intriguing complex phases including a binary decagonal phase,[13] and an as yet undetermined structure at the Al$_3$Co composition, rendering them a fertile ground for atomistic simulations. Second, ab $initio$ results have recently become available for some hypothetical structural-energy differences in this system, which enable us to test the potentials. Finally, because Co is a small atom, our approximation of ignoring the d hopping is probably better justified than in early transition metals. We use the potentials to evaluate the relative energies of a large number of competing crystal structures in this system at varying compositions. The results are remarkably consistent with the observed low-temperature phases. We analyze the stability of the complex phases in terms of features in the pair potential, and find that they are stable primarily because they have the nearest-neighbor bonding lengths that are preferred by the potentials. Finally, we analyze the systematics of the medium-range order in the complex phases, and find that the observed correlations are consistent with a minimum that we find in the Co-Co potential at 4.4 Å.

II. METHODOLOGY FOR POTENTIALS

The calculation of the pair potentials is based on a model Hamiltonian H involving a band of nearly free sp electrons and localized d states, having the following form:

$$H = H^{1el} + H^{ee} + H^{ii} . \tag{1}$$

The one-electron part has the following form:

$$H^{1el} = \sum_k \epsilon_k |k\rangle\langle k| + \sum_i \sum_{m=-2}^{2} \epsilon_d |d,m,i\rangle\langle d,m,i|$$

$$+ \sum_i \sum_{km} [V_{kim}|k\rangle\langle d,m,i| + \text{H.c.}]$$

$$+ \sum_j \sum_{k,k'} V_{kk'j}|k\rangle\langle k'| . \tag{2}$$

The summation $\sum_i$ is over all the transition-metal sites, and the summation $\sum_j$ is over all the Al and transition-metal sites. In the order of presentation, the various terms in Eq. (2) are as follows: (a) one-electron energy terms for the sp electrons, (b) on-site orbital energies for the d electrons, (c) hybridization terms which scatter d electrons into sp states, and vice versa, and (d) pseudopotential terms which scatter plane waves into each other.

Beyond H^{1el}, H^{ee} and H^{ii} contain the Coulombic electron-electron and ion-ion interactions, respectively. The former are treated approximately by the use of an appropriate dielectric function, and the latter are treated by direct summation on the basis of the Born-Oppenheimer approximation.

The functional forms of the terms in H^{1el} are as follows. The sp one-electron energies have the free-electron form

$$\epsilon_k = \hbar^2 k^2 / 2m , \tag{3}$$

with the bottom of the sp band chosen as the energy zero. The parameter ϵ_d defines the d-band center, and its value will be discussed below. The hybridization terms have the form used in Ref. 9,

$$V_{kim} = V_0(k/k_0)^2 \exp(-k/k_0) Y_{2m}(\theta_k, \phi_k) \exp(-i k \cdot R_i) , \tag{4}$$

which contains V_0 and k_0 as parameters to be fixed. Here R_i is the position of the ith transition-metal atom. The pseudopotential on a given Al or transition-metal site has the Ashcroft empty-core form[14]

$$V_{ps}^j(r) = \begin{cases} 0 & \text{for } r < r_c \\ -Z_j e^2 / r & \text{for } r \geq r_c , \end{cases} \tag{5}$$

which leads to the matrix elements

$$V_{kk'j} = \frac{1}{\Omega} \frac{4\pi Z_j e^2}{|k-k'|^2} \cos(|k-k'|r_c) \exp[-i(k-k') \cdot R_j] \tag{6}$$

or

$$V_j(q) = \frac{1}{\Omega} \frac{4\pi Z_j e^2}{q^2} \cos(q r_c) \tag{7}$$

with Ω the volume of the crystal. Here, the parameters to be obtained (for both Al and the transition metal T) are the charge Z and the core radius r_c.

The values of these parameters for the Al-Co system are given in Table I. The value of 3 for Z_{Al} is standard, and the assumed value of 1.5 for Z_{Co} corresponds roughly to sp-electron counts obtained in ab $initio$ electronic-

TABLE I. Parameters in the calculation of pair potentials.

Z^{Al}	Z^{Co}	k_F	r_c^{Al}	r_c^{Co}	k_0	V_0	ϵ_d
3.0	1.5	1.749 Å^{-1}	0.558 Å	0.62 Å	0.79 Å^{-1}	29.31 eV	11.36 eV

structure calculations.[15] These free-electron valences, together with the compositions and lattice parameters of the various observed structures, lead straightforwardly to values of k_F. We find that the values of k_F for Al and the existing structures are quite similar, as indicated in Table II. We choose the k_F of Al in this paper, since there is no ambiguity about the Al valence number, and this choice is correct for the Al-rich limit and therefore useful for considering dilute solid solutions of Co in Al. The energy corrections due to the differences in k_F will be discussed later. r_c^{Al} is obtained by fitting to the *ab initio* value of the fcc-bcc energy difference in Al,[16] and the value of r_c^{Co} is taken[17] from Ref. 15. The parameters ϵ_d, k_0, and V_0 characterizing the d states are obtained from partial moments of the electron density of states for a single Co impurity in Al, using the procedure described in Ref. 9. A simple test of the choice of r_c^{Al} is to calculate the band gap of fcc Al at $\frac{1}{2}(100)$. With our choice of r_c^{Al} we get $E_g = 0.085$ Ry, via the standard result $E_g = 2V(100)$. This is in good agreement with the *ab initio* result of 0.077 Ry in Ref. 18.

The Hamiltonian is solved approximately and transformed into a pair-potential description, using a combination of a Green's function methodology and perturbation theory. For a system described by a Hamiltonian H, we define a time-independent one-electron Green's function

$$G(E+is) = \frac{1}{E+is-H} , \qquad (8)$$

where $s = 0^+$ is an infinitesimal which we will take to zero in the end. If $\{|\alpha\rangle\}$ is any complete orthonormal set of states, then the density of states projected on a particular state $|\alpha\rangle$ is

$$\rho(\alpha,E) = -\frac{1}{\pi}\text{Im}\langle\alpha|G(E)|\alpha\rangle . \qquad (9)$$

For the case where $\{|\alpha\rangle\}$ is the continuous real-space set $\{|\mathbf{r}\rangle\}$, we have

$$\rho(\mathbf{r},E) = -\frac{1}{\pi}\text{Im}\langle\mathbf{r}|G(E)|\mathbf{r}\rangle . \qquad (10)$$

The total charge density at a given point $\mathbf{r}$ in real space is

$$\rho(\mathbf{r}) = \int_{-\infty}^{\epsilon_F} dE\,\rho(\mathbf{r},E) , \qquad (11)$$

and the total density of states at a given energy E is

TABLE II. Fermi wave vectors for fcc Al and Al-Co compounds.

	fcc Al	Al$_9$Co$_2$	Al$_{13}$Co$_4$	Al$_5$Co$_2$
k_F (Å^{-1})	1.749	1.747	1.702	1.765

$$\rho(E) = \int d\mathbf{r}\,\rho(\mathbf{r},E) . \qquad (12)$$

The types of terms that are present in the Al-Al, Al-T, and T-T pair potentials are indicated in Table III. We first consider the problem of a single d shell in a uniform electron gas (no pseudopotential yet). Via the Green's function methodology, we find that this has a spherically symmetric charge density $\rho_d(\mathbf{r})$ given by Eq. (11) using the appropriate Green's function. We then again use the Green's function methodology to calculate pair potentials for interacting d shells. Consider the problem of two d shells in a uniform electron gas. Their effective interaction (absent in the Al-T and Al-Al potentials), which is mediated by the free-electron states, has the following form:

$$V_2^{d,d'}(R) = \int_{-\infty}^{\epsilon_F} (E-\epsilon_F)\Delta\rho(E)dE , \qquad (13)$$

where $\Delta\rho$ is the difference between the density of states of two interacting d shells and the superposition of the densities of states of two isolated d shells. As is indicated in Fig. 1, the physics underlying this interaction is basically the formation of a bond charge at a distance halfway between the two T atoms. The figure shows schematically the calculated charge density along a line connecting atoms 1 and 2 (indicated by curve A in frame a). It is greater than that corresponding to the superposition of two atomic charge densities. The difference charge density (given in frame b) is strongly peaked halfway between the atoms. The maximum value of the difference charge density is quite small in comparison with the average charge density (less than 3%, but exaggerated in Fig. 1), but because the difference density has a large spatial extent perpendicular to the bond axis, this effect can still lead to a strong pair potential. It is important to note that this pair potential includes only the *indirect* interaction between the d shells, mediated by the electron gas. Direct interactions between the d shells are not included at this point. This limits the applicability of the potentials to fairly low transition-metal concentrations, and also tends to make the method more applicable to late transition metals, where the d shells are smaller.

We then turn on V_{ps} perturbatively. The interaction between pseudopotentials on different sites gives, in com-

TABLE III. Contributions to the pair potentials.

	Al-Al	Al-Co	Co-Co
(A) $\rho_d(1)\rho_d(2)$	No	No	Yes
(B) $V_{ps}(1)\rho_{ps}(2)$	Yes	Yes	Yes
(C) $V_{ps}(1)\rho_d(2)$	No	Yes	Yes

A: $\rho_d(1+2)$
B: $\rho_d(1)+\rho_d(2)$

$V_{ps}(1)$ $\rho_{ps}(2)$

$\rho_d(1+2)-(\rho_d(1)+\rho_d(2))$
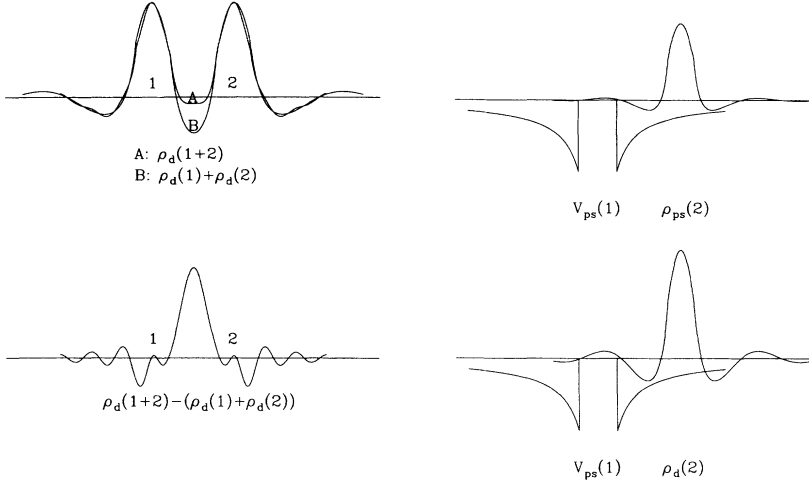
$V_{ps}(1)$ $\rho_d(2)$

FIG. 1. Schematic plots of the three contributions to the pair potentials.

bination with the direct ion-ion Coulomb interaction, the familiar screened Coulomb interaction:

$$V_2^{ps,ps'}(R)=Z_1Z_2e^2/R+\Omega^2$$
$$\times \int \frac{d\mathbf{q}}{(2\pi)^3e^2}\exp(i\mathbf{q}\cdot\mathbf{R})$$
$$\times V_{ps}^{(1)}(q)V_{ps}^{(2)}(q)\chi(q)/\epsilon(q) ,\qquad(14)$$

where the electron gas susceptibility χ and the dielectric screening function ϵ are taken from Ref. 19, which takes into account the local field corrections. As is indicated in Fig. 1(c), and can be easily shown by a Fourier transformation, this part of the potential may be written in the form

$$V_2^{ps,ps'}(R)=\int d\mathbf{r}\, V_{ps}(\mathbf{r})\rho_{ps}(\mathbf{r}-\mathbf{R}) ,\qquad(15)$$

where $\rho_{ps}(\mathbf{r})$ is the pseudopotential-induced charge density in real space, including the ionic charge. Because of the Fermi-surface induced oscillations in ρ_{ps}, $V_2^{ps,ps'}$ also has long-range oscillations.

The interaction $V_2^{ps,d}$ between pseudopotential on one site and the d-shell charge density on another T site is obtained by first-order perturbation theory in V_{ps}:

$$\Delta E^{(1)}= \sum_{\substack{\nu \\ E_\nu\leq\epsilon_F}} \langle\nu|V_{ps}|\nu\rangle$$
$$= \sum_{\substack{\nu \\ E_\nu\leq\epsilon_F}} \langle\nu|\sum_{k,k'}V_{kk'}|k'\rangle\langle k|\nu\rangle$$
$$= \sum_{k,k'} V_{k,k'} \sum_{\substack{\nu \\ E_\nu\leq\epsilon_F}} \langle k|\nu\rangle\langle\nu|k'\rangle$$
$$= \sum_{k,k'} V_{k,k'}\rho_{k'k}=\mathrm{Tr}(V\rho)=\int d\mathbf{r}\, V_{ps}(\mathbf{r})\rho(\mathbf{r}) .\qquad(16)$$

Thus we obtain a pair potential that is closely analogous to Eq. (15) for $V_2^{ps,ps'}$:

$$V_2^{ps,d}=\int d\mathbf{r}\, V_{ps}(\mathbf{r})\rho_d(\mathbf{r}-\mathbf{R}) ,\qquad(17)$$

where ρ_d is the d-shell charge density induced by the hybridization terms; it is obtained via the Green's function methodology. By interchanging the factors in the integrand, we obtain similarly $V_2^{d,ps}$. These potentials are present only for atom pairs containing at least one transition metal. The form in Eq. (17) for $V_s^{ps,d}$ is exact to first order in the pseudopotential. It ignores the effects of the pseudopotential on the shape and magnitude of ρ_d, which appear first in second order. To evaluate $V_s^{ps,d}$, we first obtain $\rho_d(\mathbf{r}-\mathbf{R})$ numerically using Eq. (22) of Ref. 9. We then Fourier transform it and use the convolution theorem to obtain $V_2^{ps,d}$.

We conclude this section with a brief discussion of the relationship of our approach to that of Moriarty.[10,11] There is a general difference of approach, in that Moriarty begins with an *ab initio* Hamiltonian, and by a successive sequence of approximations obtains a description in terms of potentials; we instead start with a simpler model Hamiltonian with analytic spatial dependences of the various couplings. We then fit some of the parameters to *ab initio* results. Regarding the specific terms in the Hamiltonian, the relationship of $V_2^{d,d}$ to Moriarty's approach has been discussed in Ref. 9; the main difference is the neglect of nonorthogonality in the present case. The $V_2^{ps,ps}$ terms are obtained from a low-order expansion of Eqs. (44) of Ref. 10, if the s-d hybridization is ignored. We believe that $V_2^{ps,d}$ is related to the Λ_{dd} term in Eq. (33) of Ref. 11. This term describes the embedding of a d shell in an electron gas which is inhomogeneous to an extent determined roughly by the $\sum_{k,k'}$ term of Eq. (35). However, we have not been able to obtain our form for $V_2^{ps,d}$ as a limiting form involving the Λ_{dd} term.

III. RESULTS

The three pieces of the potential for Co-Co pairs are illustrated in Fig. 2. We note that at distances greater than 3 Å $V_2^{d,d'}$ is by far the strongest. The asymptotic form[9] of this part of the potential is

$$V_2^{d,d'}(R)\propto E_F(2l+1)^2\cos[2k_FR-\delta(N_d)]/R^3 .\qquad(18)$$

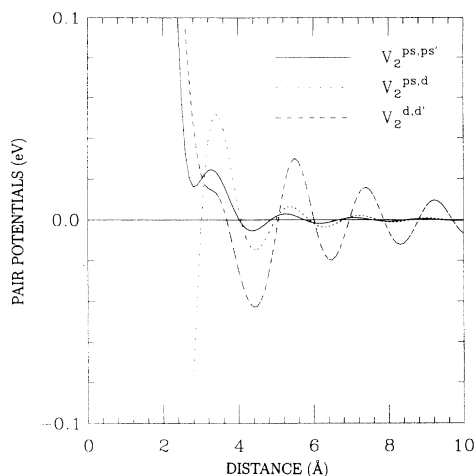We note that unlike the $V_2^{ps,ps'}$ term, there is no factor of

FIG 2. The three pieces of potential for Co-Co pairs.

a weak pseudopotential in this expression, explaining why this part of the potential is so much stronger than $V_2^{ps,ps'}$. $V_2^{ps,ps'}$ provides a strongly repulsive contribution at small distances, which may be expected to determine the minimum allowed Co-Co separation. The behavior of $V_2^{ps,d}$ is basically intermediate between that of $V_2^{d,d'}$ and $V_2^{ps,ps'}$.

The complete potentials $V_2 = V_2^{d,d'} + V_2^{ps,ps'} + V_2^{ps,d} + V_2^{d,ps}$ are plotted in Fig. 3 for Al-Al, Al-Co, and Co-Co pairs. As expected, the Co-Co potential dominates at large distances, because of $V_2^{d,d'}$. All three of the potentials have a sharp repulsive part inside the preferred nearest-neighbor separation. The Al-Al potential has a shelflike feature near the nearest-neighbor separation of 2.8 Å, which has been shown by previous calculations.[20] The Al-Co and Co-Co potentials both have quite short nearest-neighbor separations, of about 2.4–2.5 Å. This is consistent with the average Al-Co bond length in the existing AlCo structures. Note that the Al-Co potential is deeper than the average of the Al-Al and Co-Co potentials, indicating a preference for unlike neighbors in
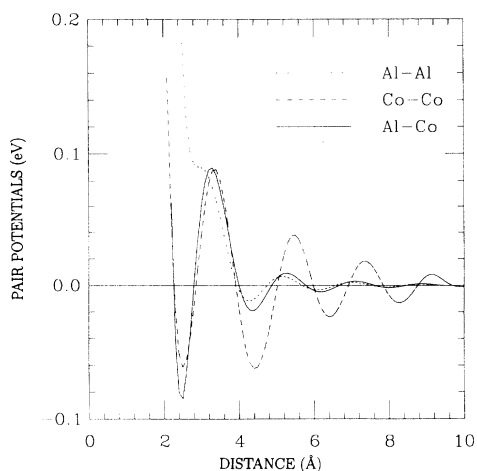
this system. This feature is consistent with both the known structures of the Al-rich ordered phases,[21] which have no Co-Co nearest neighbors, and with *ab initio* calculations[22] of Ising-type couplings for a hypothetical fcc-based Al-Co system, which yielded antiferromagnetic-sign nearest-neighbor couplings. Notice that the energy penalty for like neighbors is associated with Al-Al neighbors, not Co-Co neighbors. According to our potentials, the reason that there are no Co-Co neighbors in the Al-rich Co compounds is that they would force the presence of energetically unfavorable Al-Al bonds.

Because our intent is to develop potentials for quasi-crystal simulations, it is appropriate to use the observed Al-Co phase diagram,[23] indicated in Fig. 4, as a calibration. As the Co concentration increases from fcc Al, the system forms three known intermetallic compounds at the Al-rich end: Al_9Co_2, $Al_{13}Co_4$, and Al_5Co_2. The structure of the Al_3Co phase[24] is not completely determined yet, and will not be discussed in this paper. The structures of these compounds are complex, in the sense that the unit cells are large and the local site environments are asymmetric. The simplest of these is the Al_9Co_2 structure, its unit cell shown in Fig. 5. Each Co atom has nine Al as nearest neighbors while the Al atoms are 9-, 10-, or 12-coordinated. The average Al-Co and Al-Al bond lengths are 2.47 and 2.84 Å, respectively.

Figure 6 shows the results of a large number of structural-energy calculations for observed and hypothetical compounds in the Al-Co system. These energies are simply sums of the pair potentials in the Al-Co compounds at volumes specified by k_F. The numerical energy values, as well as "Strukturbericht" (where available) and "Pearson" symbols for the crystal structures, are given in Table IV. The energies are given relative to a composition-weighted average of the fcc Al and Cu_3Au-structure Al_3Co energies. We emphasize that our pair potentials can be used only to evaluate energies that occur at fixed average electron density. The average electron density enters the calculation of ρ_d, $V_2^{d,d'}$, and the electron gas response function χ. In principle, plots to examine structural stabilities such as Fig. 6 should contain free energies at fixed temperature and pressure. Since we are only interested in the zero-temperature phase diagram, we should in principle plot the structural energies at fixed pressure. However, our potentials are only applicable to fixed volume. Since the existing AlCo compounds have volumes per atom which are different from the one we use to calculate the potentials, corrections due to volume differences should be accounted for. We estimate the energy drops of the compounds when their optimal volumes are reached by using the bulk modulus of Al. The energy correction is less than 0.005 eV/atom for Al_9Co_2 and Al_5Co_2, and is less than 0.02 eV/atom for $Al_{13}Co_4$. These are much smaller than the absolute structural energies of the compounds and will not affect the basic features of the phase diagram. Thus the estimated energy corrections are not included in Fig. 6. The quantities plotted in Fig. 6 are still not exactly the structural energies of the AlCo compounds, since only pair interactions are included. The one-body energy terms which depend on the electron density are left out.
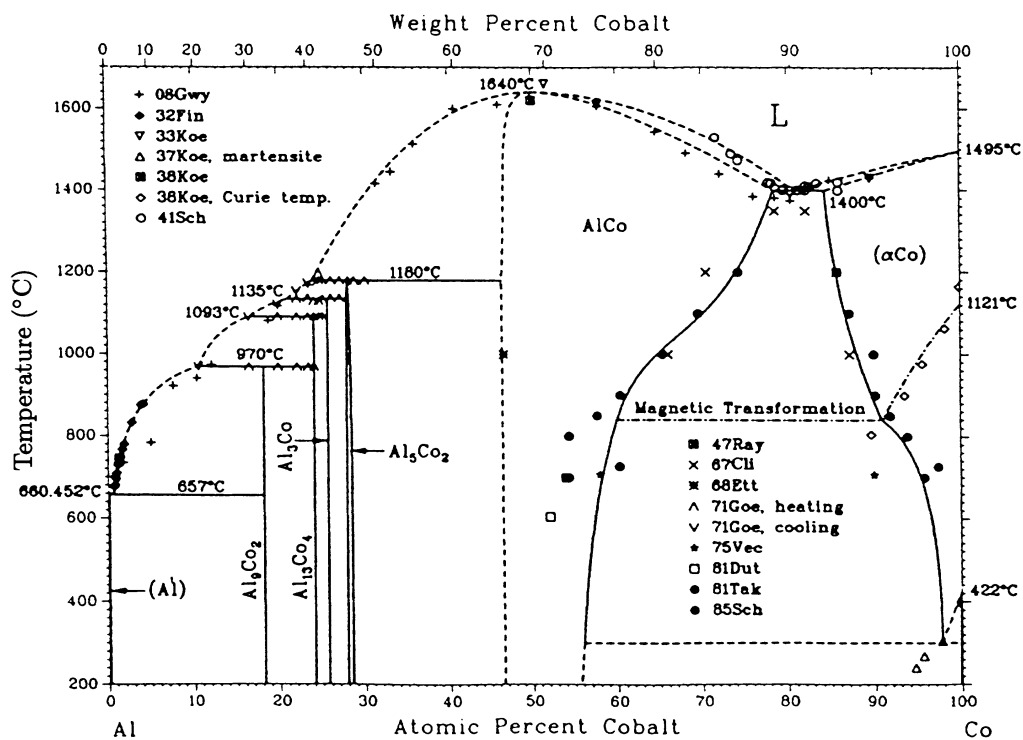

FIG. 3. Complete pair potentials for the Al-Co compounds.

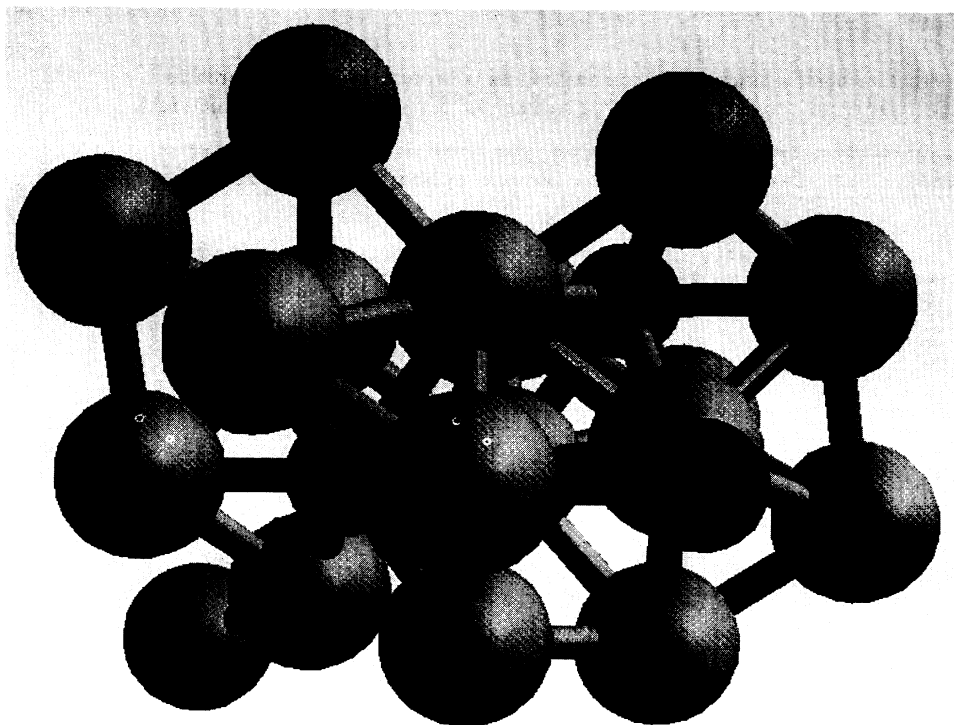FIG. 4. Al-Co phase diagram. Taken from Ref. 21.

FIG. 5. Atomic structure of Al_9Co_2. Darker and smaller spheres represent Co atoms. Nearest-neighbor bonds are denoted by cylinders.
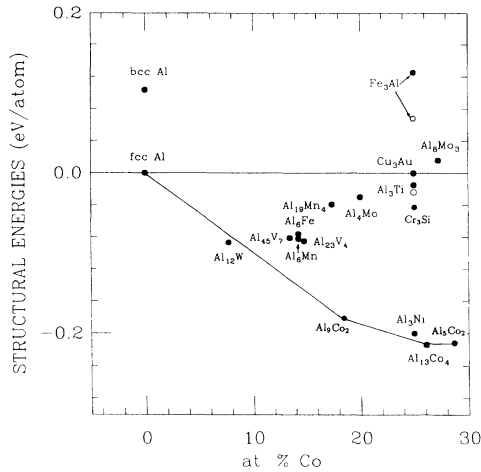
FIG. 6. Structural energies for some of the Al-Co compounds. All numbers are relative to the tie line between fcc Al and Cu_3Au. The two open circles for Al_3Ti and Fe_3Al structures are *ab initio* results (Ref. 25). In the $Al_{13}Co_4$ structure, there are vacancies and partial occupations in the Al sites, making the true Co concentration 26.3%, as indicated in the figure.

However, the concentration dependence of the one-body terms is linear at fixed electron density, since the one-body energy of a particular atom type depends only on the background electron density. Energy terms that are linear as a function of concentration have no effect on a phase diagram, since they simply correspond to shifts of the chemical potentials of the constituents. Therefore, the composition dependence of the one-body terms will have no impact on the structural energies.

We evaluate our potentials by comparison both with *ab initio* structural energies, where available, and with the experimental phase diagram. *Ab initio* results are avail-

able for only the Al_3Ti-Cu_3Au and Fe_3Al-Cu_3Au energy differences[25] for Al_3Co [in addition to the bcc-fcc energy difference for Al (Ref. 16) which was used as a fitting property]. The Al_3Co composition calculations utilized the augmented-spherical-wave method.[26] Both of the Al_3Co values, indicated by open circles, are obtained reasonably well by the potentials. The Al_3Ti-Cu_3Au energy difference measures primarily the long-range part of the potential; the Fe_3Al-Cu_3Au energy difference has substantial contributions from short-range packing effects because of the change from bcc to fcc packing. Therefore, the consistency with the *ab initio* results speaks favorably for both the long- and short-range parts of the potentials. We can also calculate the stability of Al_9Co_2 relative to fcc Al and Al_5Co_2. This is defined as

$$\Delta E = E(Al_9Co_2) - E(Al_5Co_2) - 4E(\text{fcc Al}) \qquad (19)$$

and with our potentials, ΔE is -0.051 eV/atom. The same quantity can also be deduced from the heats of formation data[27] for Al_9Co_2 and Al_5Co_2. It turns out to be -0.038 eV/atom, again in fair agreement with our result.

We are not in a position to compute the entire phase diagram, but the results in Fig. 6 predict exactly the ordered compounds that form, with the exception of $Al_{12}W$ structure, which is predicted to form but does not. In a total-energy picture such as Fig. 6, the stable compounds correspond to downward-pointing "cusps" in the lines connecting the lowest-energy structures. The energy favoring the complex $Al_{13}Co_4$ structure relative to the nearly isocompositional simple Cu_3Au structure is quite large, over 0.2 eV/atom. The stability of the complex structures is mainly due to short-range bonding constraints. This can be seen with the help of Fig. 7(a), which gives histograms of the Al-Co pair spacings in the Al_9Co_2, $Al_{13}Co_4$, and Cu_3Au structures, along with the

TABLE IV. Crystal structure nomenclature and numerical values of structural-energy differences. Energies measured in eV relative to composition-weighted average of fcc Al and Cu_3Au-structure Al_3Co.

Structure	Co at. %	Strukturbericht	Pearson symbol	Energy/atom
fcc Al	0	$A1$	$cF4$	0
bcc Al	0	$A2$	$cI2$	+0.103
$Al_{12}W$	7.69		$cI26$	−0.087
$Al_{45}V_7$	13.46		$mC104$	−0.081
Al_6Mn	14.29		$oC28$	−0.082
Al_6Fe	14.29		$oC28$	−0.076
$Al_{23}V_6$	14.81		$hP54$	−0.085
$Al_{19}Mn_4$	17.39		$cP138$	−0.039
Al_9Co_2	18.18		$mP22$	−0.1795
Al_4Mo	20.00		$mC30$	−0.030
Cr_3Si	25.00	$A15$	$cP8$	−0.043
Al_3Ni	25.00		$oP16$	−0.206
Al_3Ti	25.00		$oP16$	−0.206
Al_3Ti	25.00	DO_{22}	$tI8$	−0.015
Cu_3Au	25.00	$L1_2$	$cP4$	0
Fe_3Al	25.00	DO_3	$cF16$	+0.125
$Al_{13}Co_4$	25.86		$mC93$	−0.214
Al_8Mo_3	27.27		$mC22$	+0.016
Al_5Co_2	28.57	$D8_{11}$	$hP28$	−0.2121
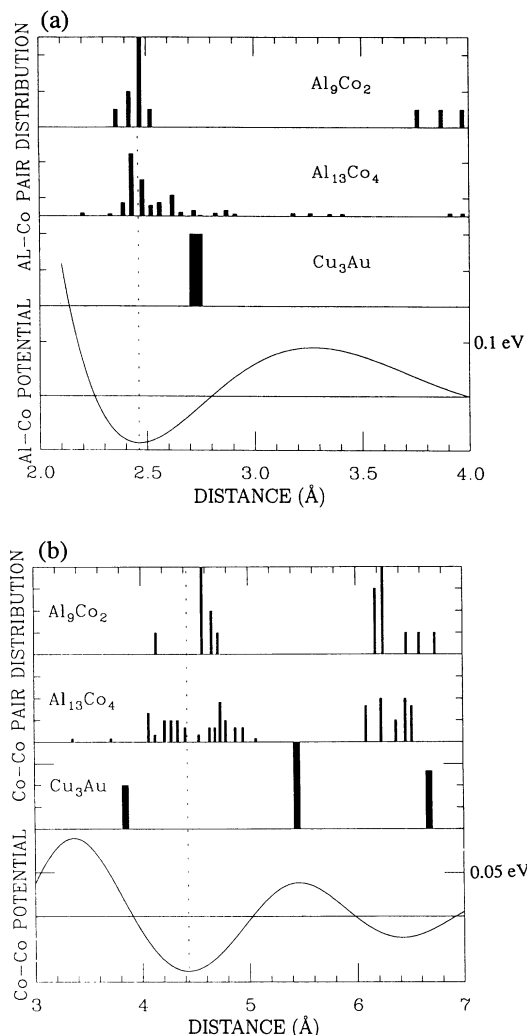
FIG. 7. Histograms of the Al-Co and Co-Co spacings in Al_9Co_2, $Al_{13}Co_4$, and Cu_3Au. Also shown are the Al-Co and Co-Co pair potentials.

Al-Co pair potential. (We find that the Al-Co contribution is the dominant one. For example, 90% of the structural energy difference between Fe_3Al and Al_3Ni comes from Al-Co potentials.) The main difference between the Cu_3Au structure on the one hand and the Al_9Co_2 and $Al_{13}Co_4$ structures on the other hand is that the first shell of neighbors is shifted in from 2.7 to about 2.45 Å. The potential is sufficiently rapidly varying that this corresponds to moving from close to a node to close to a minimum. By having only nine Al neighbors for Co in the complex structures, it is possible to have these neighbors at a short distance without forcing the Al neighbors themselves to be unphysically close. Since there are roughly two Al-Co nearest-neighbor bonds per atom in the complex $Al_{13}Co_4$ structure, and the depth of the potential is about 0.1 eV, placement of all the Al-Co spacings at the pair-potential minimum would correspond to an energy reduction of about 0.2 eV per atom, as indicated in Fig. 6.

Another smaller contribution to the stability of the complex structures comes from the second minimum in the Co-Co pair potential, at 4.4 Å. As Fig. 7(b) shows, the Co-Co spacings in the complex structures cluster around this minimum, while those in the Cu_3Au structure are at a node of the potential. This stabilizes the complex structures, but the effect is smaller than the nearest-neighbor Al-Co effect, since the 4.4-Å minimum is shallower and broader than the nearest-neighbor one. However, it may well be that the 4.4-Å minimum is an important factor in distinguishing between different complex structures.[28] For example, the Al_9Co_2 structure has a lower energy than the complex $Al_{19}Mn_4$ structure, partly because the Co-Co spacings in the $Al_{19}Mn_4$ structure are shifted out to about 4.7 Å.

IV. CONCLUSION

The main result of the above is that we have developed a viable methodology for calculating potential-energy functions in Al-rich transition-metal compounds, which includes the dominant electronic effects as well as the "classical" hard-core repulsion effects. The comparison with both *ab initio* structural-energy results and the observed phase diagram is quite encouraging. We feel that the potentials are sufficiently accurate to be used in simulations of structural properties of aluminides of late transition metals. In order to extend the range of applications of these types of potentials, at least two extensions are necessary. First, in order to go to earlier transition metals, and to higher transition-metal concentrations, it will be necessary to include the direct interactions between the d shells. Formally, this involves only a slight modification to the methodology for $V_2^{d,d'}$. However, it will lead to an additional set of parameters in the potentials. Also, at high transition-metal concentrations, it is not at all clear that the interaction energies can be described by pair potentials at all. The second extension is to find a way to go beyond a pair-potential description, and thus get around the constant-volume constraint. This would allow the treatment of defects such as surfaces, which are beyond the realm of applicability of the present potentials. We do not see a straightforward way of going beyond the pair-potential description. However, recent work[29] on elemental transition metals has shown that it is possible to transform a "constant-volume" methodology into one having the "embedded-atom" format. We hope that this may be possible in the case of the aluminides as well.

*Present address: Division of Engineering, Box D, Brown University, Providence, RI 02912.

†Present address: Metals and Ceramics Division, Oak Ridge National Laboratory, P.O. Box 2008, Oak Ridge, TN 37831.

[1] D. Shechtman, I. Blech, D. Gratias, and J. W. Cahn, Phys. Rev. Lett. **53**, 1951 (1984).

[2] A. P. Tsai, A. Inoue, and T. Masumoto, Jpn. J. Appl. Phys. **26**, L1505 (1987).

[3] A. P. Tsai, A. Inoue, and T. Masumoto, J. Mater. Sci. Lett. **7**, 322 (1988).

[4] K. H. Kuo, D. S. Zhou, and D. X. Li, Philos. Mag. Lett. **55**, 33 (1987).

[5] M. S. Daw and M. I. Baskes, Phys. Rev. B **29**, 6443 (1984).

[6] K. W. Jacobsen, J. K. Norskov, and M. J. Puska, Phys. Rev. B **35**, 7423 (1987).

[7] A. Zangwill and A. C. Redfield, J. Phys. F **18**, 1 (1988).

[8] A. E. Carlsson, Phys. Rev. B **43**, 12 176 (1991).

[9] J. Zou and A. E. Carlsson, Phys. Rev. B **47**, 2961 (1993).

[10] J. A. Moriarty, Phys. Rev. B **38**, 3199 (1988).

[11] J. A. Moriarty, Phys. Rev. B **5**, 2066 (1972).

[12] W. A. Harrison, in *Pseudopotentials in the Theory of Metals* (Benjamin, New York, 1966).

[13] X. L. Ma and K. H. Guo, Metall. Trans. **23A**, 1121 (1992).

[14] N. W. Ashcroft, Phys. Lett. **23**, 48 (1966).

[15] J. M. Wills and W. A. Harrison, Phys. Rev. B **28**, 4363 (1983).

[16] S. Ogut and K. M. Rabe (unpublished).

[17] Attempts were made to determine the core radius of Co pseudopotentials r_c^{Co} by fitting to existing *ab initio* structural energy differences between competing AlCo structures. They failed due to the insensitivity of structural energies to r_c^{Co} since r_c^{Al} dominates the energies of Al-rich AlCo compounds.

[18] V. L. Moruzzi, J. F. Janak, and A. R. Williams, in *Calculated Electronic Properties of Metals* (Pergamon, New York, 1978).

[19] S. Ichimaru and K. Utsumi, Phys. Rev. B **24**, 7385 (1981).

[20] L. Dagens, M. Rasolt, and R. Taylor, Phys. Rev. B **11**, 2726 (1975).

[21] See, P. Villars and L. D. Calvert, *Pearson's Handbook of Crystallographic Data for Intermetallic Phases* (American Society for Metals, Metals Park, Ohio, 1986).

[22] A. E. Carlsson, Phys. Rev. B **40**, 912 (1989).

[23] A. J. McAlister, Bull. Alloy Phase Diagrams **10**, 646 (1989).

[24] T. Geodecke, Z. Metallkd. **62**, 842 (1971).

[25] J. Zou and A. E. Carlsson (unpublished).

[26] A. R. Williams, J. Kübler, and C. D. Gelatt, Phys. Rev. B **19**, 6094 (1979).

[27] R. Hultgren, P. D. Desai, D. T. Hawkins, M. Gleiser, and K. K. Kelley, *Selected Values of the Thermodynamic Properties of Binary Alloys, Part I* (American Society for Metals, Metals Park, Ohio, 1973).

[28] J. Zou and A. E. Carlsson, Phys. Rev. Lett. **70**, 3748 (1993).

[29] J. A. Moriarty and R. Phillips, Phys. Rev. Lett. **66**, 3036 (1991).

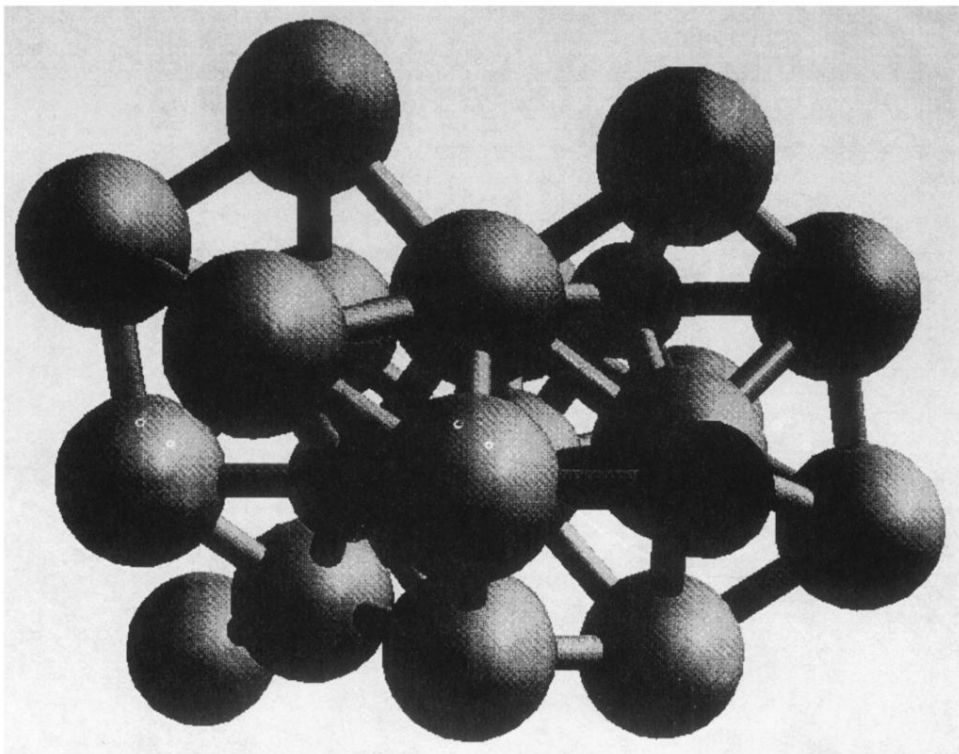FIG. 5. Atomic structure of Al_9Co_2. Darker and smaller spheres represent Co atoms. Nearest-neighbor bonds are denoted by cylinders.